

Rock magnetic investigation of possible sources of the Bangui magnetic anomaly

Ouabego^{1,2}, M., Quesnel^{2*}, Y., Rochette², P., Demory², F., Fozing³, E.M., Njanko³, T., Hippolyte², J.-C., Affaton², P.

1 – Geosciences Laboratory, Bangui University, Bangui, Centrafrican Republic

2 – Aix Marseille University, CNRS, IRD, CEREGE UM34, 13545 Aix-en-Provence, France

3 – Environmental Geology Laboratory, Dschang University, BP67, Dschang, Cameroon

*Corresponding author :

Quesnel Yoann

Aix Marseille University, CNRS, IRD, CEREGE UM34, 13545 Aix-en-Provence, France

Ph.: +33 442971590

Fax: +33 442971595

Email: quesnel@cerege.fr

Abstract

The Bangui Magnetic Anomaly (BMA) is the largest lithospheric magnetic field anomaly on Earth at low latitudes. Previous studies investigated its geological source using constraints from satellite and ground magnetic field measurements, as well as from surface magnetic susceptibility measurements on rocks from the Panafrican Mobile Belt Zone (PMBZ). Here we combine magnetic field data modelling and rock magnetic property measurements (susceptibility and natural remanent magnetization, NRM) on many samples from this PMBZ and the surrounding formations. It reveals that NRM is a significant component of the total magnetization (Mt) of the BMA source, which reaches 4.3 A/m with maximum thicknesses of

38 and 54 km beneath the western and eastern parts of the BMA. Only the isolated and relatively thin banded iron formations and some migmatites show such Mt values. Thus we suggest that the thick BMA source may be composed either by overlapped slices of such metamorphic rocks, or by an iron-rich mafic source, or by a combination of these two geological structures.

Keywords: Bangui magnetic anomaly, magnetization, geological source, modelling, banded iron formation

1 – Introduction

Located in Centrafrican Republic, the Bangui Magnetic Anomaly (BMA) is one of the largest lithospheric magnetic field anomaly on Earth, prominent even at satellite altitude. Different models have been proposed concerning its geological source. First, Regan and Marsh (1982) suggested that a geological metamorphic process affected the entire crust of this area during the Panafrican orogenesis, creating physical property contrasts between cratonic regions and collisional belts. Ravat (1989) reinforced this model but suggested an additional concentrated near-surface ore-like body (see also Ravat et al., 2002 and Langel and Hinze, 1998). This shallow body could correspond to the remains of an iron meteorite that fell in this area during the Proterozoic era (Girdler et al., 1992; see also De et al., 1998 and Gorshkov et al., 1996). Shock, thermal and/or chemical remanent magnetizations acquired during and after the impact should have led to this highly-magnetized body. However, the impact hypothesis is less suitable since the impactor material does not survive in significant amount in large craters and thus cannot contribute to such a large magnetic anomaly (Koeberl, 1998). Furthermore no shock remanent magnetization was observed on the rock samples from this area (Marsh, 1977). All these studies lack of constraints from magnetic property measurements on the

corresponding rocks of this area. Here we combined rock magnetic measurements with magnetic field anomaly modelling in order to investigate the possible source of the BMA.

In the first section, we summarize the geological context of the Centrafrican Republic, especially in our studied area. Then, the BMA is introduced before the description of the methods used. The next section details the results of magnetic property measurements and BMA modelling over the studied area. The last section corresponds to a discussion on the origin of the BMA, in the context of the general challenge involved in understanding large and deep crustal anomalies using limited access to rock samples (e.g. Frost and Shive, 1986; McEnroe et al., 2004, Rochette et al., 2005).

2 – Geological context

Central Africa is a key area of the African Plate since it constitutes the transition between several old cratons (Figure 1a,b). This transition corresponds to several orogenic belts such as the Panafrican belt (Nickles, 1952; Gérard, 1958; Black, 1966; Mestraud, 1971; Alvarez, 1992, 1995; Rolin, 1995a,b). These belts are mobile zones of the Panafrican Orogenesis at 600 ± 100 Ma (Kennedy, 1964; Rocci, 1965; Black, 1966). During this orogeny plate movements closed oceanic areas leading to a belt of suture zones around the cratons in the African regions of Gondwana. Our study area corresponds to Central Africa (Cameroon, Centrafrican Republic, Chad and Congo) where the West-African and Congolese cratons are separated by the Precambrian and Palaeozoic Oubanguides mobile zones (Figure 1b; Nickles, 1952; Gérard, 1958; Mestraud, 1971; Rolin, 1995b). Four geological domains are observed in this area from the rare outcrops of the Archean terranes (about 3.5 Ga), the Eburnean basement (2.4-2.2 Ga), the Neoproterozoic Panafrican cover (600 Ma) and the post-Panafrican domain (Figure 1b,c). We focus our study on the southwestern part of the Centrafrican Republic (Figure 1c) where the Oubanguides Panafrican Belt borders to the

north the Congo craton. Syn- and post-glacial Marinoen sediments cover the Neoproterozoic layers (Alvarez, 1999; Rolin, 1995a). A collision of an oceanic plate led to the presence of metamorphic rocks that were sampled in this area (granulites, quartzites including Banded Iron Formations (BIF), migmatites, orthogneisses, metabasalts, metasediments and metaperidotites). All metamorphic grades are found from granulite to green schist. The whole sequence was remobilized during the Panafrican orogenesis in nappes (formation 6 on Figure 1c) cut by N140 and N70-trending reverse faults (Figure 1c).

3 – Geophysical context

The western part of Central Africa shows one of the most prominent large-scale magnetic anomaly on Earth: the Bangui magnetic anomaly (BMA; Figure 2). It corresponds to a multipolar magnetic anomaly with a negative central lobe and two positive north and south lobes (all are located south to the geomagnetic equator). It reaches about 800 km of N-S wavelength and about 1000 nT of amplitude at ground level. Its E-W axial extension also reaches about 700 km. Near the magnetic equator and in the sub-tropical zone, this is the largest magnetic field anomaly. Here we use the anomaly field from the Magnetic Field model 7 (MF7; modified from the MF6 of Maus et al. (2008)) and downward continued to near the Earth's surface (2.5 km altitude – but this is considered as the 'satellite' signal in the following). This model was derived using 2007-2010 magnetic data from the low-Earth orbit CHAMP satellite. It resolves the crustal magnetic field anomalies with wavelengths larger than 300 km, for example the long-wavelength part of the BMA.

Ground magnetic data with a heterogeneous spatial resolution are also used in this study. They were acquired by LeDonche and Godivier (1962) in Centrafrican Republic and Chad (therefore no ground data were acquired at the southern lobe of the BMA). The published maps are of the horizontal and vertical components of the total magnetic field, as

well as the declination. To recover the total magnetic field (TF) anomaly, they subtracted the corresponding International Geomagnetic Reference Field (IGRF) model values from TF values. We preferred to apply the Definitive Geomagnetic Reference Field (DGRF) model for year 1960 (coefficients published in Finlay et al. (2010)) to derive the anomaly. It should be noted that the TF anomaly values are close to the horizontal component anomaly values, as expected for such low latitudes near the magnetic equator. The shape of the BMA differs between the satellite data map and the ground data map. Indeed the latter reveals that the western limit of the negative lobe of the satellite-derived anomaly is more heterogeneous at ground level, with a local positive E-W elongated central anomaly nearby (5°N, 17°E) surrounding by local negative lobes south and north. Also, the E-W transition between the central negative lobe and the northern positive one on the satellite-derived anomaly map is about 0.3° north than the same transition on the ground data map. This could indicate that the main source body lies in the lower and middle crusts but that only several branches of this source may really reach the upper crust. The negative lobe of the anomaly is more intense (-1000 nT) on the ground data map than on the satellite anomaly map (-400 nT). It is also very well correlated to a negative Bouguer gravimetric anomaly (data from Boukéké et al., 1995) of -125 mGal, indicating that the magnetization contrasts in the crust of this area may be correlated to rock density contrasts from the same source region.

4 – Methods

4.1 – Magnetic anomaly modelling

To investigate the magnetic properties of the BMA source, we first used a modelling method with the observed (ground as well as satellite-derived) magnetic and ground gravimetric anomaly fields. The GM-SYS module of the GEOSOFT Oasis montaj software was used. Gravity (Boukéké et al., 1995) and magnetic anomaly data along the NW-SE

profiles shown on Figure 2 were considered. The geometry of the different geological layers was constrained by 1) our own field observations (only near the western profile), 2) data from previous geological maps (Rolin, 1995a), and 3) gravimetric and magnetic anomaly data. Along the western profile, only the surface geology, ground magnetic and gravimetric data really constrained the model, because the satellite-derived magnetic signal cannot reproduce the short wavelengths observed at 2.5 km altitude. On the other hand, along the long eastern profile, too few surface observations, probably representing very 'local' anomalies, exist to consider the interpolated profile as a reasonable constraint. The directions of the remanent magnetization vector of the source body were initially set to the 2011 and 1960 Bangui magnetic field directions (Finlay et al., 2010) for modelling of satellite-derived and ground data, respectively, but could vary if necessary during the inversion. The main aim of the magnetic modelling was to infer the approximate range of total magnetization (Mt) of the most magnetic formation beneath the BMA under the assumptions of induced magnetization constraint and of a source model geometry able to fit the data whatever the location (western or eastern profiles).

4.2 – Sampling and rock magnetic measurements

Over 50 large hand samples were obtained in the area of Figure 1c, during several field missions. Sampling was designed to cover all lithologies and degrees of metamorphism observed in this area. Petrography was determined using thin sections and, in some cases, X-ray diffraction and chemical analysis. Low field magnetic susceptibility measurements were carried out using SM30 susceptibility meter (ZH Instruments) for large samples and KLY2 susceptibility meter (AGICO) for small samples. Mass susceptibility χ was calculated using the weight of the samples. For remanence and further rock magnetic measurements a first set of samples (chosen to be representative of all lithologies) was completed by all samples with

high susceptibility remaining in the collection: therefore the proportion of high susceptibility samples is higher in the studied set. A total of 22 samples were thus fully investigated magnetically. The Natural Remanent Magnetization (NRM) as well as saturation isothermal remanent magnetization (SIRM) acquired at 1 T were measured using a spinner magnetometer Minispin (Molspin) for large samples. In one case NRM was analysed by alternating field demagnetization of a small sample using a superconducting rock magnetometer 760R (2G enterprises). To characterize the magnetic minerals, thermomagnetic curves were acquired using a MFK1 susceptibility meter (AGICO) with CS3 furnace (up to 650°C under argon atmosphere), ambient temperature hysteresis measurements were performed with a vibrating sample magnetometer Micromag 3900 (PMC) and its cryostat allowed measuring low temperature remanent magnetizations.

To compare with the magnetic properties of somewhat similar formations within the Panafrican belt, we analysed susceptibility data from East Cameroon (Betaré Oya area, see Figure 1a,b and Kankeu et al., 2009) as well as West Cameroon (after Njanko et al., 2012 and ongoing magnetic anisotropy investigations of amphibolites and granitoids). Some samples from W Cameroon were also measured for rock magnetic properties.

Mass normalized rock magnetic measurements were used to evaluate in-situ M_t (in A/m) of the sampled formations using the following formula:

$$M_t = \rho (NRM + \chi H)$$

with ρ the rock density (2.7 g/cm³ for all rocks – a typical value for deep continental crust, see Table 1 - except itabirites which were assumed to be 3.2 g/cm³) and H the present magnetic field intensity in Bangui (33.6 μ T, i.e. 26.8 A/m). Using field intensities at the dates of the discussed magnetic field surveys makes negligible changes. This formula assumes that

the induced and remanent magnetization components are colinear. Thus the resulting M_t values computed with this equation will be maximum values. The Koenigsberger ratio ($Q = \text{NRM} / \chi H$) was also calculated.

5 – Results

5.1 – Magnetic anomaly modelling

The best models to represent the crustal magnetization and density variations beneath the western and eastern BMA profiles are shown in Figure 3, and the parameters associated to each layer are indicated in Table 1. For the most magnetic layer, using a shape similar than the one shown in Figure 3 but with different M_t value and associated thickness, a M_t of 4.3 A/m indeed results in the best predictions of the data along both eastern and western profiles (see Table A1, Figures A1 and A2 in Supplementary Material). Only the 2.5 km-altitude satellite-derived magnetic data of the western profile and the ground magnetic data of the eastern profile are not well predicted, as expected (see explanations in Section 4.1). The resulting magnetization directions are similar to the input values. Similarly to the results of previous BMA modelling studies, the superficial geological layers seem to be weakly magnetized. With the selected shape, the top of the main magnetic source (layer 1) is 9 km deep beneath the short western profile, 5 km deep beneath the long eastern profile. The total magnetic thickness of this layer reaches 38 and 54 km beneath the western and eastern profiles, respectively, even if significant lateral N-S thickness variations are observed beneath the western profile (Figure 3). This confirms that a huge amount of strongly magnetized rocks is preserved in the crust of Centrafrican Republic, even beneath the sampled area near Bangui. The gravity and magnetization contrasts in the models are similar to those of the model proposed by Marsh (1977) and Regan and Marsh (1982) using satellite data only and modelling the whole BMA. In particular, the magnetic source seems to be less dense (density

contrast of about -0.03 g/cm^3) than the deep non-magnetic surrounding rocks (mainly layer 3), but denser ($> 0.2 \text{ g/cm}^3$) than the superficial non-magnetic formations (not considered in model (b) of Figure 3). Note that a small relief of the Moho is necessary to completely explain the shape of the gravity signal along the two profiles. Concerning the 4.3 A/m magnetization intensity for the most magnetic layer of the best model, using only induced magnetization would require a rather unrealistically high k of $16 \cdot 10^{-2} \text{ SI}$ for the rocks of the studied area. Therefore we arbitrarily separated this M_t value into a NRM of 4 A/m and a volumic susceptibility k of 10^{-2} SI (Table 1).

5.2 – Magnetic property measurements

Table 2 shows the magnetic properties of the 22 studied samples. Most of our strongly magnetic samples have Koenigsberger ratios (Q) larger than 1 (minimum values 0.3), stressing the importance of not relying only on susceptibility measurements. Only two samples corresponding to migmatite (8576) and itabirite (8603), have M_t over 4.3 A/m , while five other samples have $0.8 < M_t < 2.3 \text{ A/m}$, from the above lithologies plus granodiorite (8632) and orthogneiss (240). Other lithologies (metaperidotites, metabasalts, granulite and non itabiritic metasedimentary rocks) have negligible M_t . The strong M_t values are coherent with the susceptibility measurements made by Marsh (1977) on outcrops from the area beneath the large Bangui magnetic anomaly, eastward from our own sampling. Those samples with the largest observed magnetic susceptibilities are itabirites from Bakala (k around 0.1 SI) and charnockites from Kaga Bandaro (k around 0.02 SI). We do not elaborate further on Marsh (1977) data obtained using a Bison large coil applied on the outcrops, as their precision and cross-calibration with our more precise data is unknown.

Hysteresis loops obtained on chips from the 6 most magnetic samples reveal 4 samples (Figure 4; including 8576) typical of multidomain magnetite $-M_{rs}/M_s < 0.02$, $B_{cr}/B_c > 5$,

226 Bcr<20 mT- and two samples (8603 and 240) typical of hematite -Mrs/Ms>0.5, Bcr/Bc≈1.3,
227 Bcr>20 mT. Hematite appears multidomain for the itabirite sample (8603) and single domain
228 for the orthogneiss (240). To confirm these identifications, we measured low temperature
229 remanent magnetizations on the two most magnetic samples (Figure 5) and high-temperature
230 susceptibility on the 4 samples showing multidomain magnetite (Figure 6). At low
231 temperature, Morin and Verwey transitions are visible on 8603 and 8576 respectively (Figure
232 5), indicating that pure hematite and pure magnetite are indeed present in these rocks.
233 Magnetite Curie point (at 580°C; Figure 6) is observed on all samples but in 8603 and 240
234 over 50% of initial susceptibility remains over 650°C, indicative of hematite that should carry
235 most of the remanence. For sample 240, this weak residual signal may also correspond to
236 instrument drift, but the previous hysteresis measurements have shown hematite.

237 For surface rock samples, the measured NRM intensities can be biased by the viscous
238 remanent magnetization (VRM) component and other possible spurious unwanted
239 magnetizations, especially lightning induced IRM that can generate anomalously high NRM
240 (Verrier and Rochette, 2002). Therefore we scaled measured NRM with saturation IRM, and
241 computed theoretical in situ NRM intensities from measured SIRM. For samples containing
242 magnetite, we applied a theoretical NRM/SIRM ratio of 2% (Gattacceca and Rochette, 2004)
243 using a thermo-remanent magnetization (TRM) in the present magnetic field in Bangui. These
244 modelled Mt values are shown in the last column of Table 2. Only two samples exhibit
245 modelled values significantly different from the value computed using our NRM and
246 susceptibility measurements: magnetite-bearing migmatite (8576) and hematite-bearing gneiss
247 (243). For the latter, modelled value is much higher, possibly due to a multicomponent IRM
248 with opposite directions. Measured value for 8576 is 3 times larger than the modelled Mt,
249 suggesting that lightning has biased our NRM measurement, although much larger
250 NRM/SIRM ratios are commonly observed for samples affected by lightning (Verrier and

Rochette, 2002). An alternative-field demagnetization experiment with REM' ratio computed following Gattacceca and Rochette (2004) does confirm that 8576 NRM is affected by lightning, with REM' peaking at 30%. For samples containing hematite (8603 and 240), the modelled Mt values (using NRM/SIRM = 50% after Kletetschka et al., 2000, and Dunlop and Kletetschka, 2001) are similar to the observed ones (30 to 50%).

Finally, we compare the magnetic properties of our samples with those measured on other rock samples from the Panafrican belt in Cameroon (Figure 7). For West Cameroon Fomopea amphibolites (Njanko et al., 2012; geographic position near 5.5N and 10E), among 16 sites (with 2 to 4 samples per sites), the maximum k is $9 \cdot 10^{-2}$ SI, with 25% of the sites above 10^{-2} SI. In the Nkambé area (6N and 10E), mostly with granitoids but also with accessory amphibolites, the maximum k is $5 \cdot 10^{-2}$ SI in both lithologies, with 16% of the over 1200 samples above 10^{-2} SI (Fozing et al., in preparation). Rock magnetic measurements, including hysteresis loops and thermomagnetic curves, have been performed on a selection of 48 samples (Table A2 of the Supplementary Material). They all show a multidomain to large pseudo-single domain magnetite signal. Modelled Mt has been computed after SIRM and susceptibility measurements (Figure 8). Only 15 samples yield values over 1 A/m, a single one being over 4 A/m (at 6.8 A/m). For those strong samples, Q ratio is always over 1 (average around 2), stressing again the need to take remanence into account, even for multidomain magnetite. For the East Cameroon study of Kankeu et al. (2009, at 5.5N and 14E), the susceptibility of 65 metasediments (schist, quartzite and gneiss) and 18 deformed granites was measured. For these two classes, the maximum k is 2 and $5 \cdot 10^{-2}$ SI, with 5 and 61% of the samples above 10^{-2} SI, respectively.

It appears from Figure 7 that the mean magnetic susceptibility distribution is roughly similar regardless of the location in the Panafrican belt, with metamorphic rocks derived from basalts and granites having the strongest magnetic susceptibilities. These histograms confirm

on a larger scale the conclusion from our samples: no surface lithologies are able to account for the BMA by induced magnetization alone (e.g. Shive, 1989). A review of the extensive magnetic anisotropy work in Panafrican intrusives from NE Brasil (e.g. Archanjo et al., 1995, 1998, 2002) confirms this conclusion. When taking into account remanence it appears that magnetite-bearing crustal rocks (granitoids and amphibolite) exceptionally reaches the BMA total magnetization (Figure 8).

6 – Discussion

These results indicate that a single lithology -hematite-bearing itabirites, i.e. BIF, interstratified with amphibolites and other metasediments- shows strong enough total magnetization M_t to be the magnetic source of the BMA ($M_t > 4.3$ A/m). Lithologies rich in multidomain magnetite (some amphibolites and granites) fail by about a factor 2 to account for the BMA, assuming no significant enhancement of NRM at depth. No magnetic field observations were made at the itabirite sampling locations (LeDonche and Godivier, 1962), but such outcrops should result in a local small-wavelength high-amplitude magnetic field anomalies. Our assumption that the deep crustal lithologies responsible for the BMA could be outcropping over the BMA relies on the possibility that some slices from these deep lithologies have been brought to the surface through orogenic processes (e.g. Rolin, 1991). Our modelling shows that the deep magnetic source seems to be less dense than the deep non-magnetic surrounding rocks (granulites?), but denser than most of the superficial non-magnetic formations (quartzites and schists). We also note the numerous reverse faults in this Panafrican belt around Bangui that witness a compressive regime which may have favored the thickening of the iron-rich formations (Figure 1c).

The total magnetization intensity and the expected volume of the geological source of the BMA are coherent with a mafic (basaltic) lower crust, as Pin and Poidevin (1987) and

Hemant and Maus (2005) suggested. This metabasalt or amphibolitic part of the Central Africa's lower crust may be the root of the migmatite basement. However, our results also suggest that BIF may compose the source of the BMA because of their magnetization. These rocks are assumed to compose about 25% of the source of the Kursk magnetic anomaly in Russia (Taylor, 1987; Ravat et al., 1993; Langel and Hinze, 1998). In such case, a positive gravimetric anomaly should be associated to the BMA, as Schmidt et al. (2007) observed on a similar geological formation in Australia (magnetization up to 100 A/m). However as itabirite can be an order of magnitude more magnetized than the BMA source, a volume occupied by a mixture of 10% itabirite (i.e. a maximum thickness of 2 km) and 90% of low density and less magnetic rock can account for the BMA without inducing a significant excess of mass. As mentioned earlier, a negative gravimetric contrast is associated to the BMA in its central part, but a positive one is found west of Bangui nearby Cameroon border (Boukéké et al., 1995), where a positive magnetic anomaly and itabirites are also observed. Finally, the combination of these two possible magnetic formations (itabirites and amphibolite) may explain the long wavelength and large intensity of the BMA.

It is interesting to note that probably all Panafrican metamorphic crustal formations, including these magnetic rocks from the lower crust, may be found on surface today in the Centrafrican Republic, while for other large magnetic anomalies like the Beattie magnetic anomaly in South Africa, the source is from the upper and middle crust but covered by the Karoo basin sediments (Quesnel et al., 2009). Two key points of our interpretation are the possible Curie isotherm -deepened in case of hematite-bearing rocks- in the Central Africa lithosphere, as well as the magnetic mineralogy that carries these strong magnetization intensities at such depth (Frost and Shive, 1986; McEnroe et al., 2004). If it is hematite, our study puts forward a candidate lithology: itabirite or BIF. If it is multidomain magnetite, then the candidate lithology has not been sampled at the surface. It should be two times richer in

magnetite than the most magnetite-rich granitic and amphibolitic samples studied so far. Such a high Fe amount should correspond to a positive gravity anomaly that is not observed. However, a “homogeneous” tectonic mixing of BIF slices, a few km thick in total, with other metasediments and a few tens of km thick series of magnetite-rich metamagmatic rocks may be the best solution to account for all geophysical data.

7 – Conclusion

Using modelling and rock magnetism constraints, we investigated the source of the BMA using samples obtained over the anomaly in Centrafrican Republic, as well as geologically related areas in Cameroon. Modelling implies a total magnetization of the order of 4 A/m on a thickness up to 54 km, possibly associated with relatively moderate density of 2.87. No surface sample can account for this magnetization based only on induced magnetization. Large enough remanent magnetization intensities are observed for only two surface samples, but lightning has affected one. This highlights the fact that modelled in-situ NRMs based on IRM and magnetic mineralogy may be a more reliable indicator in magnetic anomaly interpretation, compared to NRM actually measured on surface samples, which can yield strongly-biased values with respect to NRM at depth.

The only remaining lithology, with NRM up to 50 A/m, is hematite-bearing itabirites (BIF) that are Neoproterozoic iron-rich metasediments. Other magmatically-derived lithologies rich in multidomain magnetite (migmatite, amphibolite, granite) can account for only a few A/m at most. We suggest that the two types of geological formation may compose the deep crust of this area and particularly the extended deep magnetic source. Further constraints given by drilling or by other geophysical methods like seismics or magnetotellurics are needed to validate (or not) this interpretation and the previously-published models. Concerning magnetics, new high-resolution ground and airborne magnetic

field measurement surveys will surely improve the characterization of this source, including its possible extensions toward the surface. In the same time, one should benefit from the upcoming SWARM satellite mission (Friis-Christensen et al., 2006) that will allow the use of lateral and vertical magnetic gradients to study such large magnetic anomalies.

Acknowledgments

The Bangui University is acknowledged for its support to this work, as well as the OSU-Institut Pytheas. We also thank the two anonymous reviewers who greatly contributed to improve the first state of this manuscript.

References

- Almeida, F.F.M., Brito Neves, B.B., de Carneiro, C.D.R., 2000. The origin and evolution of the South American Platform. *Earth Sci. Rev.*, 500, 77–111.
- Alvarez, P., 1992. Répartition de la sédimentation dans le golfe Protérozoïque supérieur du Schisto-calcaire au Congo et au Gabon: Implications en Afrique centrale. *Palaeogeogr. Palaeoclimat. Palaeoecol.*, 96, 281-297.
- Alvarez, P., 1995. Evidence for a Neoproterozoic carbonate ramp on the northern of the Central African craton: relations with the Late Neoproterozoic troughs. *Rundschau*, 84, 636-648.
- Alvarez, P., 1999. Un segment proximal de rampe carbonatée d'âge protérozoïque supérieur au Nord du craton d'Afrique Centrale (Sud-Est de la République Centrafricaine). *J. Afr. Earth Sci.*, 23, 263-266.

374 Archanjo, C.J., Launeau, P., Bouchez, J.-L., 1995. Magnetic fabric vs. magnetite and biotite
 375 shape fabrics of the magnetite-bearing granite pluton of Gameleiras (Northeast Brazil).
 376 *Phys. Earth Planet. Int.*, 89, 63-75.

377 Archanjo, C.J., Macedo, J.W.P., Galindo, A.C., Araujo, M.G.S., 1998. Brasiliano crustal
 378 extension and emplacement fabrics of the mangerite-charnockite pluton of Umarizal,
 379 North-east Brazil. *Precambr. Res.*, 87(1-2), 19-32.

380 Archanjo, C.J., Trindade, R.I.F., Bouchez, J.-L., Ernesto, M., 2002. Granite fabrics and
 381 regional-scale strain partitioning in the Serido belt (Borborema Province, NE Brazil).
 382 *Tectonics*, 21, doi:10.1029/2000TC001269.

383 Black, R., 1966. Sur l'existence d'une orogénie riphéenne en Afrique occidentale. *C.R. Acad.*
 384 *Sci. Paris*, 262, D, 1046-1049.

385 Boukéké, D.-B., Legeley-Padovani, A., Poudjom-Djomani, Y.-H., Foy, R., Albouy, Y., 1995.
 386 Gravity map of Central African Republic: Bouguer anomalies. ORSTOM, Institut
 387 français de recherche scientifique pour le développement en coopération. Carte
 388 1/6000000, Lever gravimétrique de reconnaissance.

389 De, S., Heaney, P.J., Hargraves, R.B., Vicenzi, E.P., Taylor, P.T., 1998. Microstructural
 390 observations of polycrystalline diamond: a contribution to the carbonado conundrum.
 391 *Earth Planet. Sci. Lett.*, 164, 421-433.

392 Dunlop, D.J., Kletetschka, G., 2001. Multidomain hematite: A source of planetary magnetic
 393 anomalies?. *Geophys. Res. Lett.*, 28, 3345-3348.

394 Ferré, E., Dereris, J., Bouchez, J.L., Lar, A.U., Peucat, J.J., 1996. The Pan-African
 395 reactivation of Eburnean and Archean provinces in Nigeria: structural and isotopic
 396 data. *J. Geol. Soc. London*, 153, 719-728.

397 Feybesse, J.L., Johan, V., Triboulet, C., Guerrot, C., Mayaga-Mikolo, F., Bouchot, V., Eko
 398 Ndong, J., 1998. The West Central African belt: a model of 2.5–2.0 Ga accretion and
 399 two-phase orogenic evolution. *Precambr. Res.*, 87, 161–216.

400 Finlay, C.C., Maus, S., Beggan, C.D., Bondar, T.N., Chambodut, A., Chernova, T.A.,
 401 Chulliat, A., Golovkov, V.P., Hamilton, B., Hamoudi, M., Holme, R., Hulot, G.,
 402 Kuang, W., Langlais, B., Lesur, V., Lowes, F.J., Lühr, H., Macmillan, S., Manda, M.,
 403 McLean, S., Manoj, C., Menvielle, M., Michaelis, I., Olsen, N., Rauberg, J., Rother,
 404 M., Sabaka, T.J., Tangborn, A., Tøffner-Clausen, L., Thébaud, E., Thomson, A.W.P.,
 405 Wardinski, I., Wei, Z. and Zvereva, T.I., 2010. International Geomagnetic Reference
 406 Field: the eleventh generation. *Geophys. J. Int.*, 183, 1216-1230.

407 Friis-Christensen, E., Lühr, H., Hulot, G., 2006. Swarm: A constellation to study the Earth's
 408 magnetic field. *Earth Planets Space*, 58, 351-358.

409 Frost, B.R., Shive, P.N., 1986. Magnetic mineralogy of the lower continental crust. *J.*
 410 *Geophys. Res.*, 91, 6513–6522.

411 Gattacceca, J., Rochette, P., 2004. Toward a robust paleointensity estimate for meteorites.
 412 *Earth Planet. Sci. Lett.*, 227, 377-393.

413 Gérard, G., 1958. Carte géologique de l'Afrique Equatoriale Française au 1/2000000. Notice
 414 explicative. Pub. DGM AEF.

415 Girdler, R.W., Taylor, P.T., Frawley, J.J., 1992. A possible impact origin for the Bangui
 416 magnetic anomaly (central Africa). *Tectonophysics*, 212, 45–58.

417 Gorshkov, A.I., Titkov, S.V., Pleshakov, A.M., Sivtsov, A.V., Bershov, L.V., 1996. Inclusions
 418 of native metals and other mineral phases into Carbonado from the Ubangi Region
 419 (Central Africa). *Geology of Ore Deposits*, 38, 114-119.

420 Hemant, K., Maus S., 2005. Geological modeling of the new CHAMP magnetic anomaly
 421 maps using a geographical information system technique. *J. Geophys. Res.*, 110,
 422 B12103, 1–23.

423 Kankeu, B., Greiling, R.O., Nzenti, J.P., 2009. Pan-African strike-slip tectonics in eastern
 424 Cameroon-Magnetic fabrics (AMS) and structure in the Lom basin and its gneissic
 425 basement. *Precambr. Res.*, 174, 258–272.

426 Kennedy, W.Q., 1964. The structural differentiation of Africa in the Panafrican (+/- 500
 427 millions years) tectonic episode. 8th ann. Rep. Res. Inst. afro Geol. Leeds Univ., U.K.,
 428 48-49.

429 Kletetschka, G., Wasilewski, P.J., Taylor, P.T., 2000. Unique thermoremanent magnetization
 430 of multidomain-sized hematite: Implications for magnetic anomalies. *Earth Planet.*
 431 *Sci. Lett.*, 176, 469-479.

432 Koeberl, C., 1998. Identification of meteoritical components in impactites. In: M.M. Grady,
 433 R. Hutchison, G.H.J. McCall, D.A. Rothery (Editors). *Meteorites: Flux with Time and*
 434 *Impact Effects*. Geol. Soc. London, Spec. Publ., 140, 133–152.

435 Langel, R.A., Hinze, W.J., 1998. The magnetic field of the Earth's lithosphere: the satellite
 436 perspective. Cambridge University Press, 429 p.

437 LeDonche, L., Godivier, R., 1962. Réseau magnétique ramené au 1^{er} janvier 1956 :
 438 République Centrafricaine, Tchad méridional. ORSTOM, Office de la recherche
 439 scientifique et technique outre mer, cartes 1/2500000, Cahiers ORSTOM /
 440 Géophysique, No 1.

441 Marsh, B.D., 1977. On the origin of the Bangui magnetic anomaly, Central African Empire,
 442 NASA Report, 63 p.

443 Maus, S., Yin, F., Lühr, H., Manoj, C., Rother, M., Rauberg, J., Michaelis, I., Stolle, C.,
 444 Müller, 2008. Resolution of direction of oceanic magnetic lineations by the sixth-

445 generation lithospheric magnetic field model from CHAMP satellite magnetic
 446 measurements. *Geochem. Geophys. Geosyst.*, 9, Q07021,
 447 doi:10.1029/2008GC001949.

448 McEnroe, S.A., Langenhorst, F., Robinson, P., Bromiley, G., Shaw, C., 2004. What's
 449 magnetic in the lower crust?. *Earth Planet. Sci. Lett.*, 226, 175–192.

450 Mestraud, J.L., 1971. Afrique centrale. In: *Tectonique de l'Afrique*. UNESCO, Paris, 461-507.

451 Nickles, M., 1952. Les formations géologiques de la cuvette tchadienne. In: *Rapport de la*
 452 *commission scientifique du Logone et du Tchad*. Paris, 13p.

453 Njanko, T., Fozing, E.M., Kwékam, M., Yakeu Sandjo, A.F., Njonfang, E., 2012. Magnetic
 454 characterization of amphibolite from the Fomopéa pluton (West Cameroon): their
 455 implication in the Pan-African deformation of the central african fold belt. *Acta*
 456 *Geologica Sinica*, 86, 1, 73-84.

457 Penaye, J., Toteu, S.F., Tchameni, R., Van Schmus, W.R., Tchakounté, J., Ganwa, A., Minyem,
 458 D., Nsifa, E.N., 2004. The 2.1 Ga West Central African Belt in Cameroon extension
 459 and evolution. *J. Afr. Earth Sci.*, 39, 159–164.

460 Pin, C., Poidevin, J.L., 1987. U-Pb Zircon evidence for a Pan-African granulite facies
 461 metamorphism in the central African Republic: A new interpretation of the high-grade
 462 series of the northern border of the Congo craton. *Precamb. Res.*, 36, 303–312.

463 Poidevin, J.L., 1991. Les ceintures de roches vertes de la République Centrafricaine
 464 (Mbomou, Bandas, Boufoyo, Bogoin): contribution à la connaissance du Précambrien
 465 du Nord du craton du Congo. PhD Thesis, Sci.Univ. Clermont-Ferrand, 440p.

466 Quesnel, Y., Weckmann, U., Ritter, O., Stankiewicz, J., Lesur, V., Manda, M., Langlais, B.,
 467 Sotin, C., Galdéano, A., 2009. Simple models for the Beattie Magnetic Anomaly in
 468 South Africa. *Tectonophysics*, doi:10.1016/j.tecto.2008.11.027.

469 Ravat, D.N., 1989. Magsat investigations over the greater African region. Ph.D. Thesis,
470 Purdue University.

471 Ravat, D.N., Hinze, W.J., Taylor, P.T., 1993. European tectonic features observed by Magsat.
472 Tectonophysics, 220, 157-173.

473 Ravat, D., Wang, B, Wildermuth, E., Taylor, P.T., 2002. Gradients in the interpretation of
474 satellite-altitude magnetic data: an example from central Africa. J. Geodyn., 33, 131-
475 142.

476 Regan, R. D., Marsh, B.D., 1982. The Bangui magnetic anomaly: Its geological origin. J.
477 Geophys. Res., 87, 1107–1120.

478 Rocci, G., 1965. Essai d'interprétation de mesures géochronologiques : La structure de l'Ouest
479 Africain. Coll. Int. Géochronol., Nancy Sci.Terre, X, 461-478.

480 Rochette, P., Gattacceca, J., Chevrier, V., Hoffmann, V., Lorand, J.P., Funaki, M., Hochleitner,
481 R., 2005. Matching Martian crustal magnetization and meteorite magnetic properties.
482 Meteorit. Planet. Sci, 40, 529-540.

483 Rolin, P., 1991. Présence d'un chevauchement ductile majeur d'âge panafricain dans la partie
484 centrale de la République Centrafricaine : résultats préliminaires. C.R. Acad. Sci.Paris,
485 315, II, 467-470.

486 Rolin, P., 1995a. Carte tectonique et géologique de la République Centrafricaine au
487 1/1.000000, ORSTOM.

488 Rolin, P., 1995b. La zone de décrochements panafricains des Oubanguides en République
489 Centrafricaine. C.R. Acad. Sci. Paris, 320, IIa, 63-69.

490 Schmidt, P.W., McEnroe, S.A., Clark, D.A., Robinson, P., 2007. Magnetic properties and
491 potential field modeling of the Peculiar Knob metamorphosed iron formation, South
492 Australia: An analog for the source of the intense Martian magnetic anomalies?. J.
493 Geophys. Res., 112, b03102-b004495.

- 494 Shive, P.N., 1989. Can remanent magnetisation in the deep crust contribute to long
495 wavelength magnetic anomalies?. *Geophys. Res. Lett.*, 16, 89-92.
- 496 Taylor, P.T., Frawley, J.J., 1987. Magsat anomaly data over the Kursk region, U.S.S.R. *Phys.*
497 *Earth Planet. Inter.*, 45, 255-265.
- 498 Toteu, S.F., Van Schmus, W.R., Penaye, J., Michard, A., 2001. New U–Pb, and Sm–Nd data
499 from North-central Cameroon and its bearing on the pre-Pan-African history of central
500 Africa. *Precambr. Res.*, 108, 45–73.
- 501 Verrier, V., Rochette, P., 2002. Estimating peak currents at Ground Lightning Impact using
502 Remanent Magnetization. *Geophys. Res. Lett.*, 29, 10.1029/2002GL015207.

515 **Figure captions**

516

517 **Figure 1:** Location (a), regional (b) and local (c) geological contexts of the studied area. In
518 (a), the black rectangle and disks correspond to the sampled areas in Centrafrican Republic
519 and Cameroon, respectively. The dotted-dashed line delineates the coastline of South
520 America, translated and rotated next to Africa. A zoom is shown in (b) where the relationships
521 between the different Archean blocks are reconstituted. Zone A corresponds to the
522 Paleoproterozoic rocks with Archean inheritances underlining the border of the mega-Congo
523 craton. Zone B are the Pan-African rocks with Paleoproterozoic inheritances. Zone C
524 represents the nappes of the 600 Ma Central African Belt. Zone D corresponds to the
525 Mesozoic sediments of the Benue trough and Zone E are the oceanic rocks. PF, Pernambuco
526 fault; ADF, Adamawa fault; TBF, Tchollire–Banyo fault; dotted-dashed lines: reconstituted
527 South America (SW one) and Africa (NE one) coastlines. This (b) regional map is modified
528 from Penaye et al. (2004), Poidevin (1991), Ferré et al. (1996), Feybesse et al. (1998),
529 Almeida et al. (2000) and Toteu et al. (2001). The dashed rectangle corresponds to the
530 Centrafrican sampled area (c), while the black disks show the approximate locations of the
531 sampled areas in Cameroon. In (c), modified from Rolin (1995a), details about the surface
532 lithology and the structural features of the studied area nearby Bangui are shown. 1, Archean
533 gneissic basement; 2, Paleoproterozoic migmatitic domain; 3, Lower-Neoproterozoic domain
534 with (a) quartzites and (b) itabirites; 4, Upper-Neoproterozoic schists; 5, Upper-
535 Neoproterozoic limestones/marbles; 6, Panafrican Gbayas Nappe with orthogneisses,
536 granulites and granites; 7, Post-Panafrican cover with sandstones and clays. Black filled
537 circles with names indicate the sampling sites.

538

Figure 2: Interpolated magnetic anomaly maps near the surface over Centrafrican Republic and Chad. On left, gridded data from the satellite MF7 model (derived from Maus et al. (2008) downward continued to 2.5 km of altitude). On right, ground magnetic data interpolated from LeDonche and Godivier (1962). The solid lines correspond to the selected profiles for modelling, while the rectangle indicates the location of Figure 1c.

Figure 3: Crustal magnetic models (bottom panels) along the NW-SE western (a) and eastern (b) profiles (top panels) shown on Figure 2. Sat, satellite-derived magnetic data; Ground, ground magnetic data; Gravi, ground gravity data (Boukéké et al., 1995); Obs, observations, Pred, predictions. For models, layer density and magnetization properties are represented by the filling color and/or pattern (see Table 1 for details). Formation 1 has a total magnetization intensity (Mt) of 4.3 A/m, which corresponds to the best model with this source geometry (see Supplementary Material).

Figure 4: Hysteresis curves (specific magnetization) of four samples. Bc, coercitive field; Ms, saturation magnetization; Mrs, remanent magnetization at saturation; Bcr, coercitive field of the remanent magnetization, derived from the back-field curve.

Figure 5: Low-temperature remanent magnetization (RM) curves for two samples (cooling and subsequent heating of a room temperature IRM), showing the Verwey (in a) and Morin (in b) transitions. For (b) is also shown the induced magnetization (IM) heating and cooling curves, measured in a 0.3 T field.

Figure 6: Effect of heating (black) and cooling (gray) on the normalized magnetic susceptibility of the same four samples as in Figure 4.

564

565 **Figure 7:** Histogram (in logarithmic representation) of k_m , the mean magnetic susceptibility,
566 for Cameroon and Centrafrican Republic (CR) rock samples.

567

568 **Figure 8:** Histogram of modelled total magnetization (Mt) derived from IRM and
569 susceptibility measurements on Panafrican magnetite-bearing rocks from Cameroon (black)
570 and Centrafrican Republic (white).

Figure 1 revised
[Click here to download high resolution image](#)

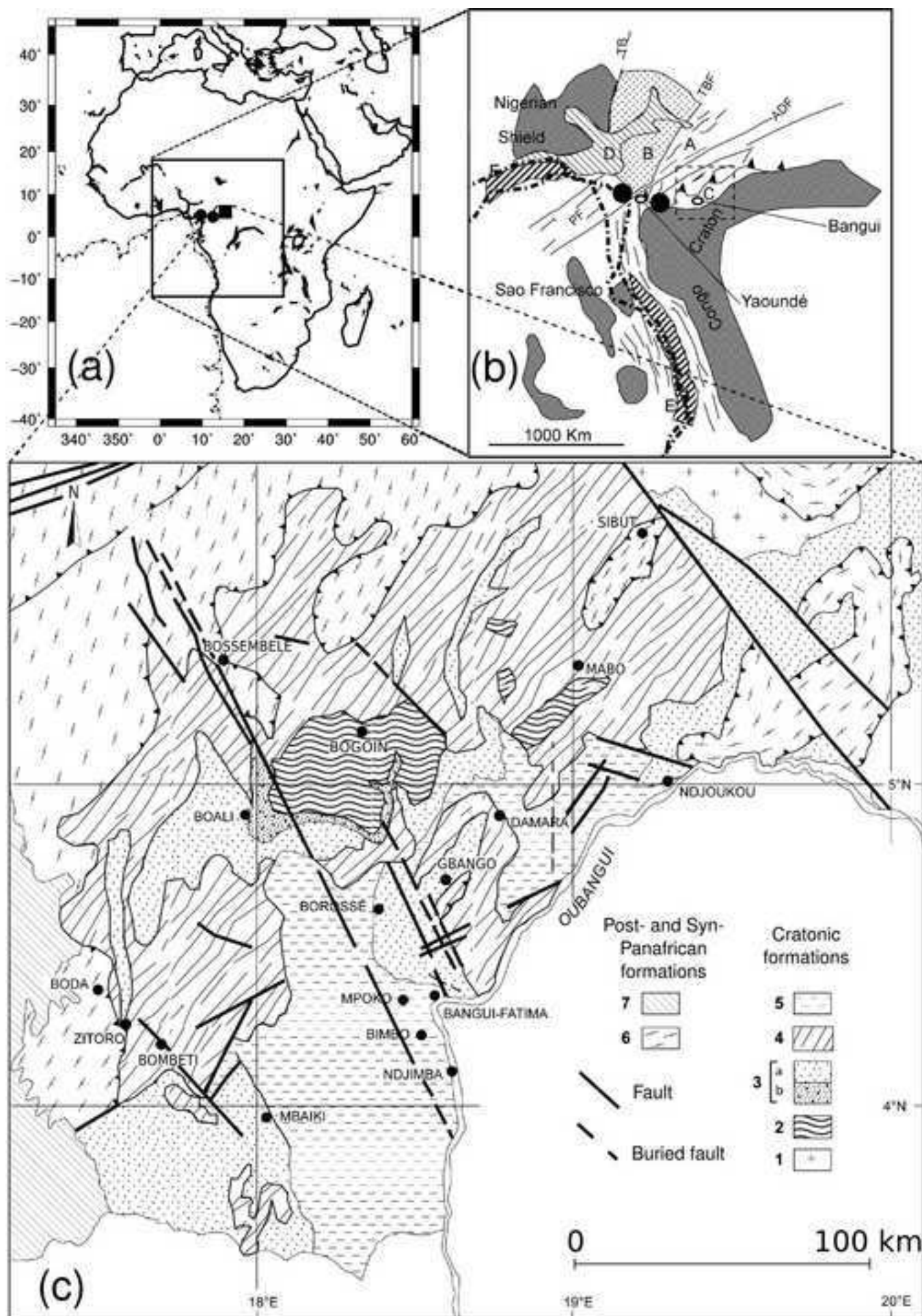


Figure 2 revised
[Click here to download high resolution image](#)

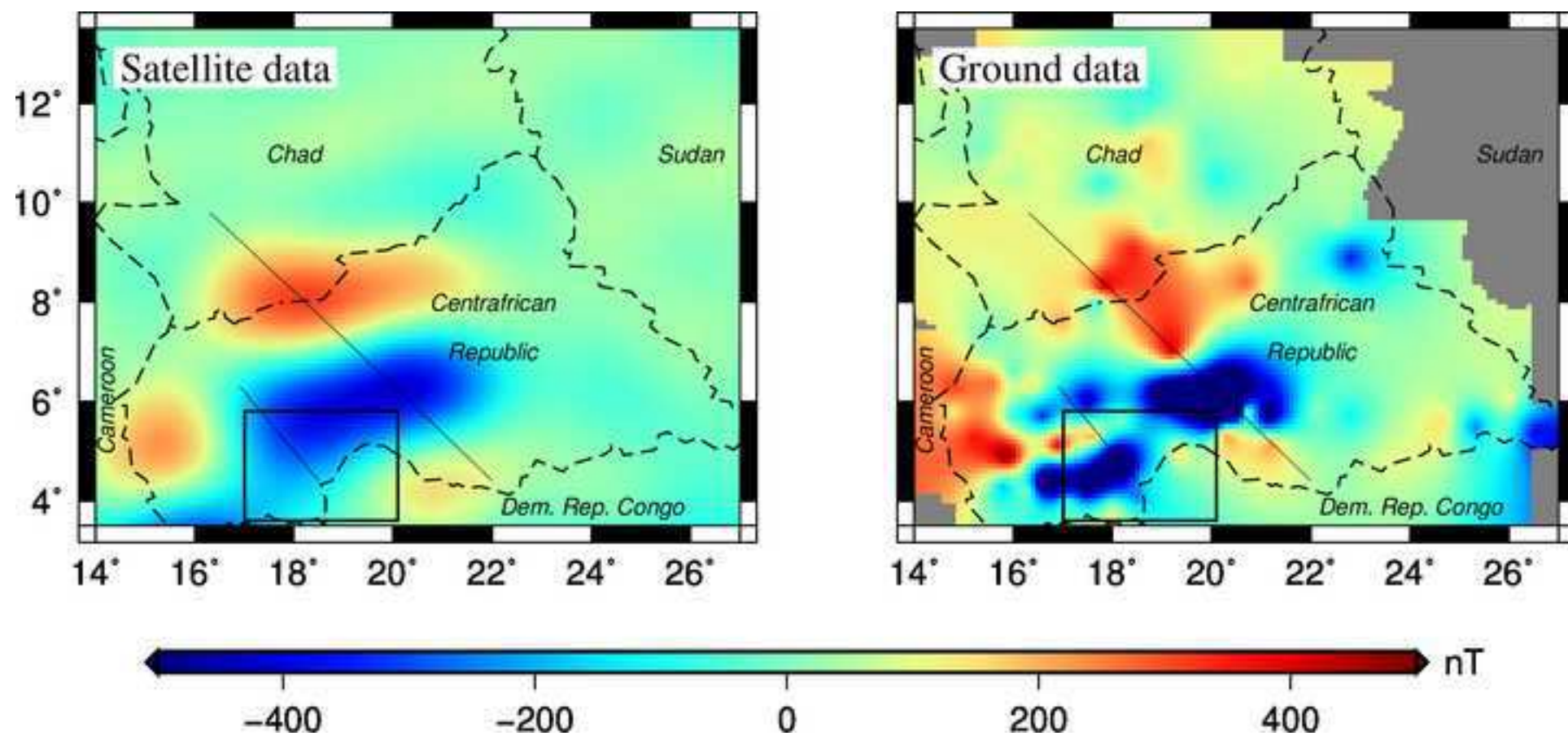


Figure 3 revised
[Click here to download high resolution image](#)

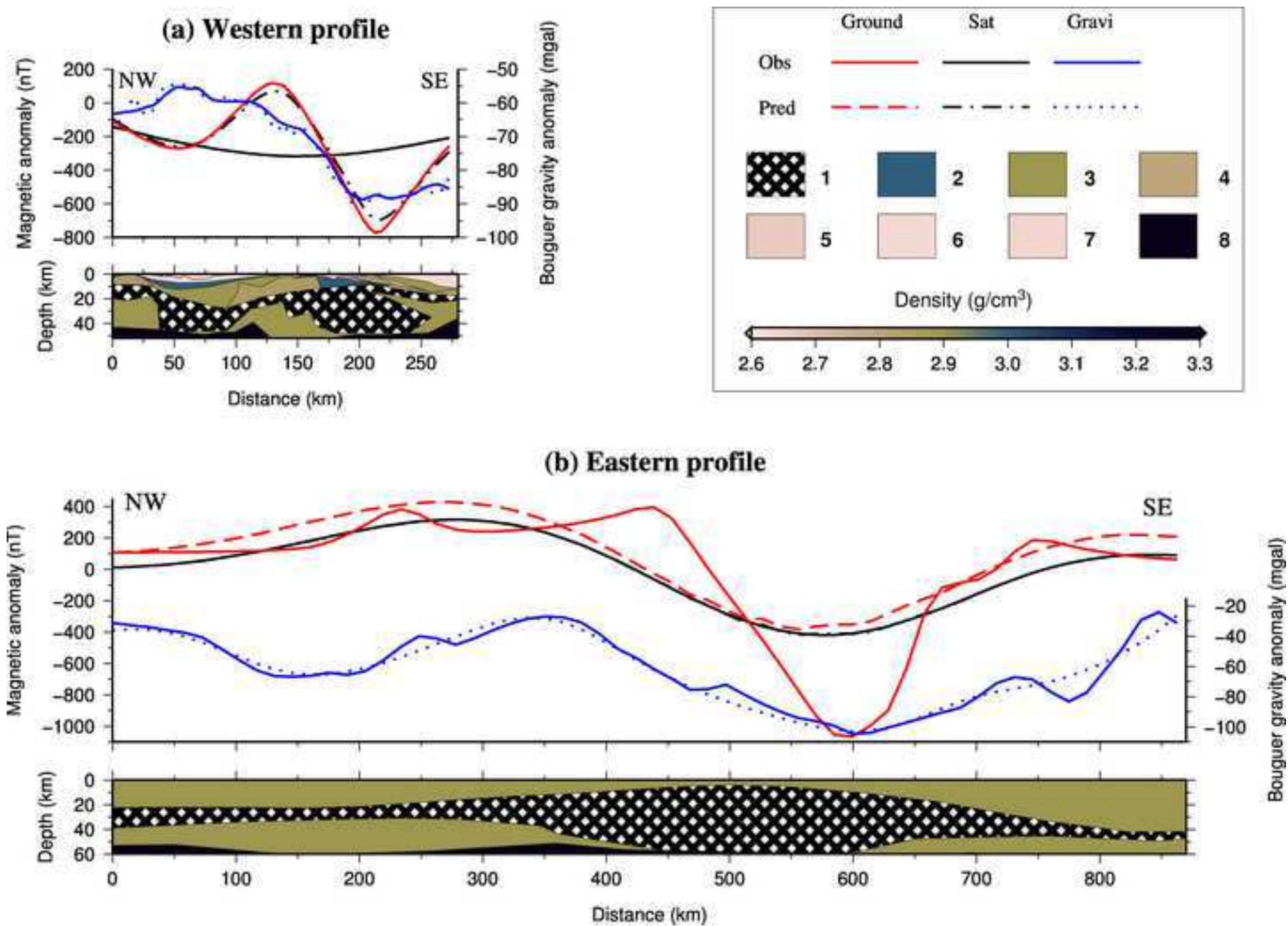


Figure 4 revised

[Click here to download high resolution image](#)

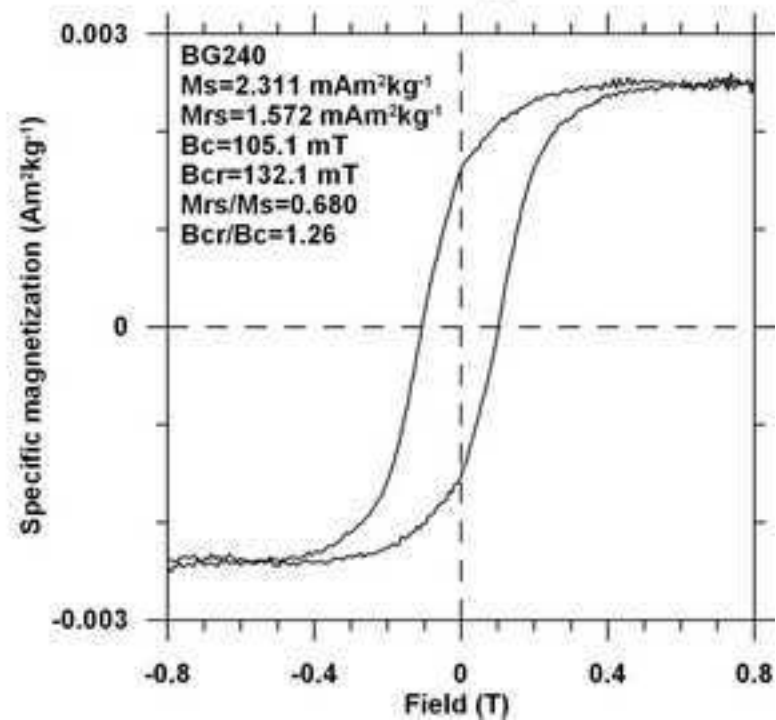
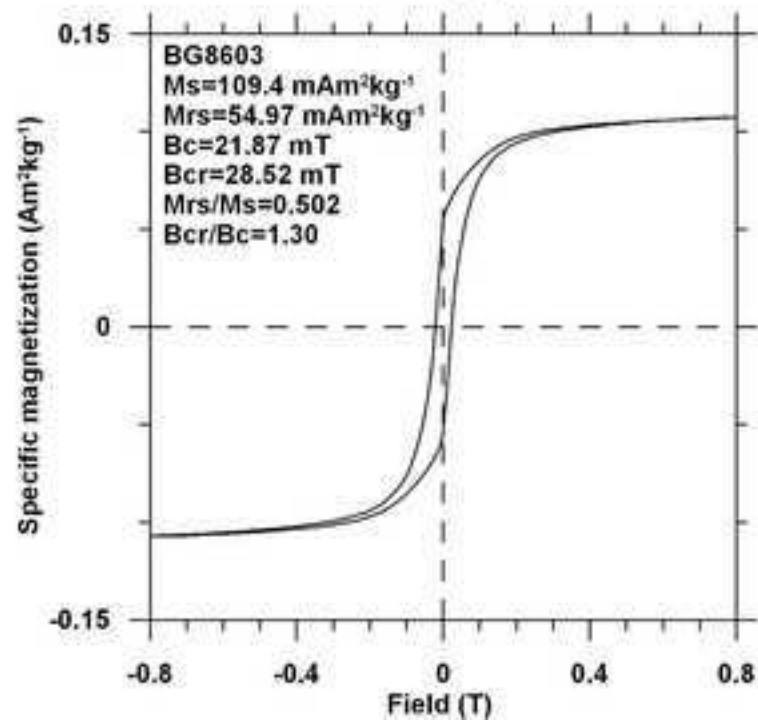
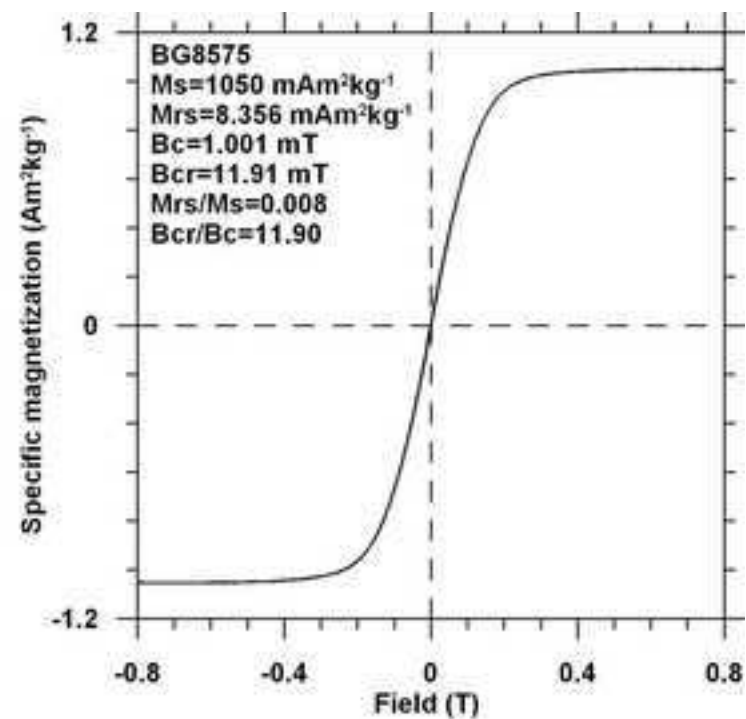
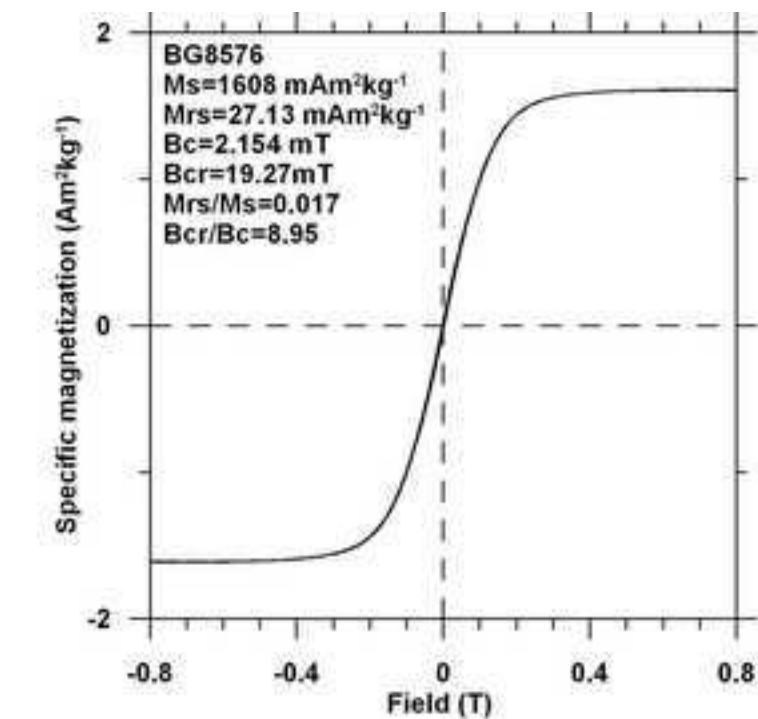


Figure 5 revised

[Click here to download high resolution image](#)

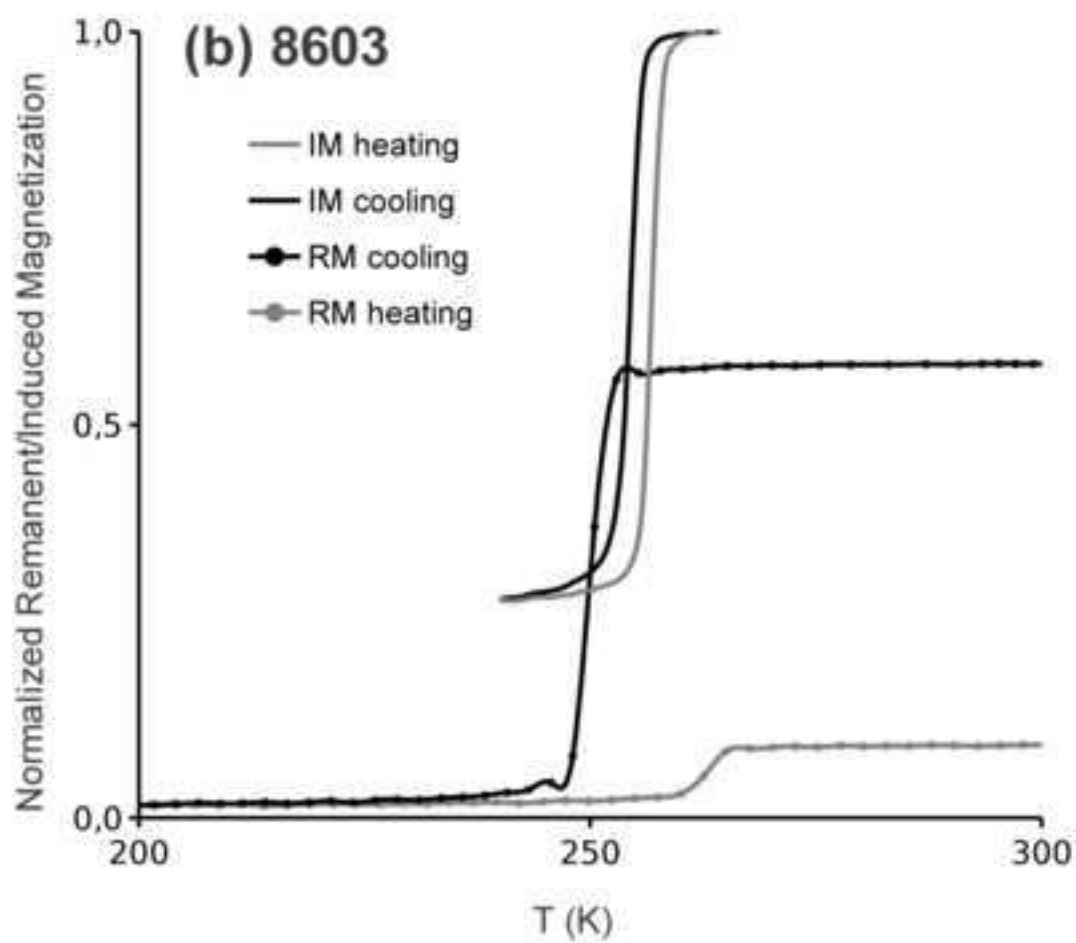
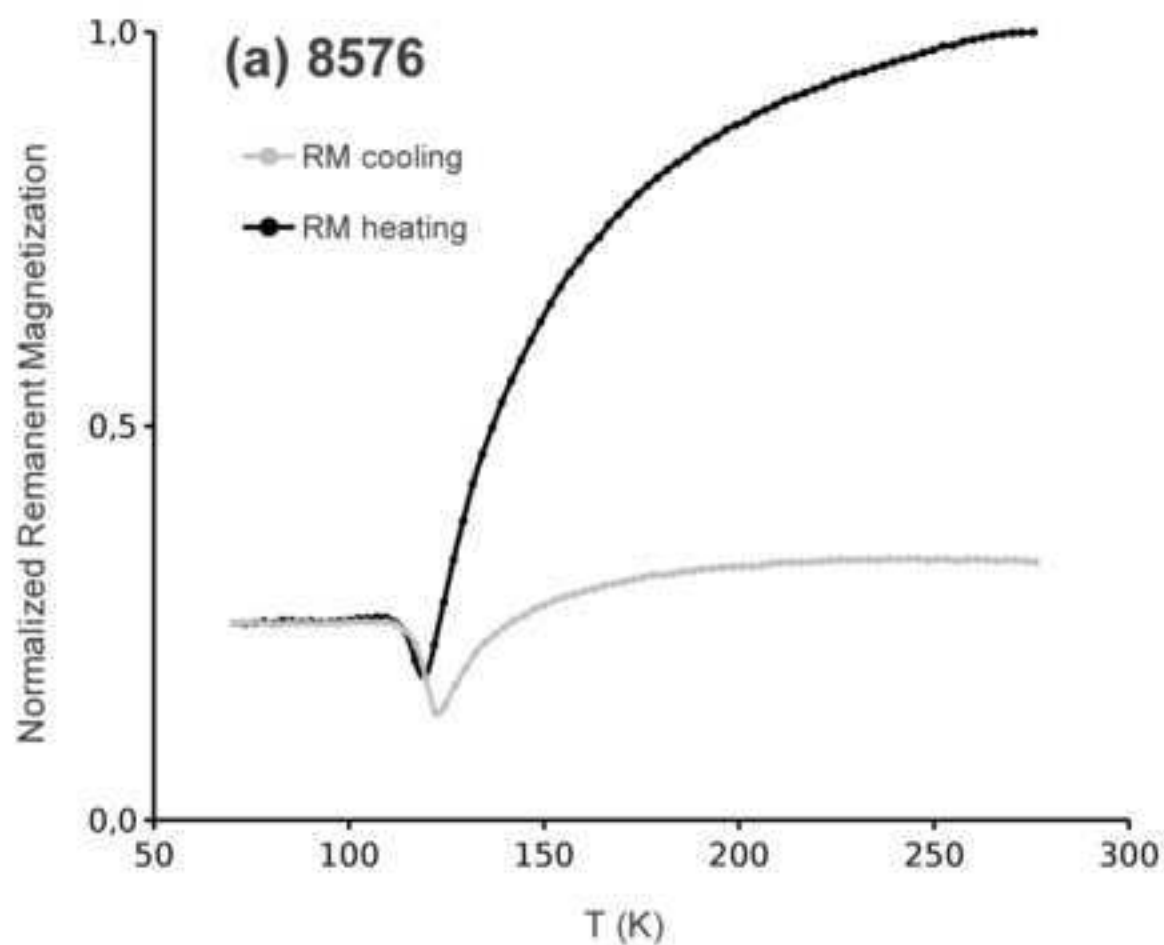


Figure 6
[Click here to download high resolution image](#)

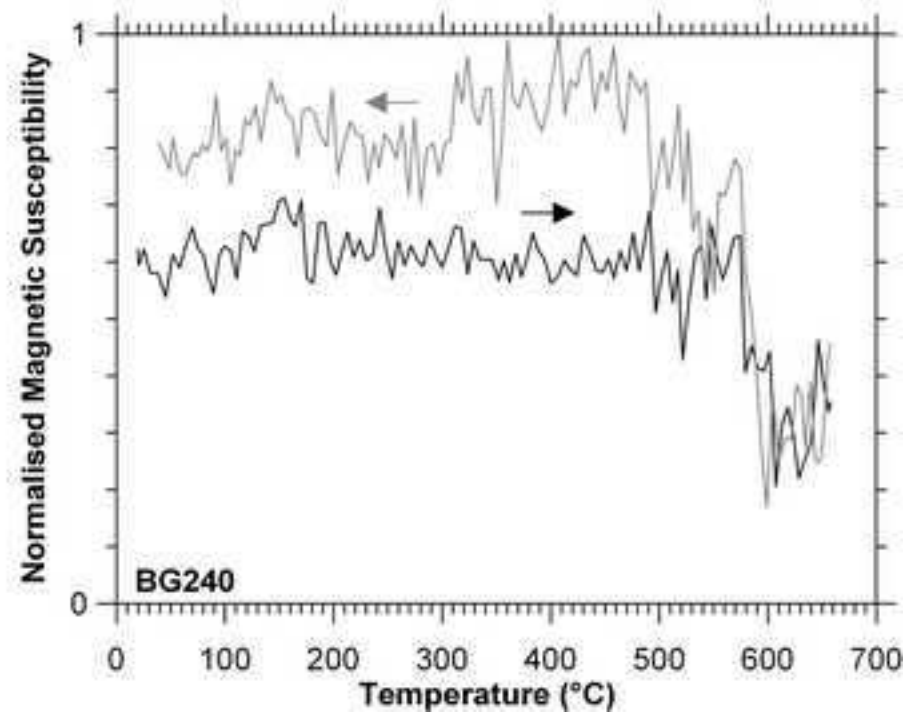
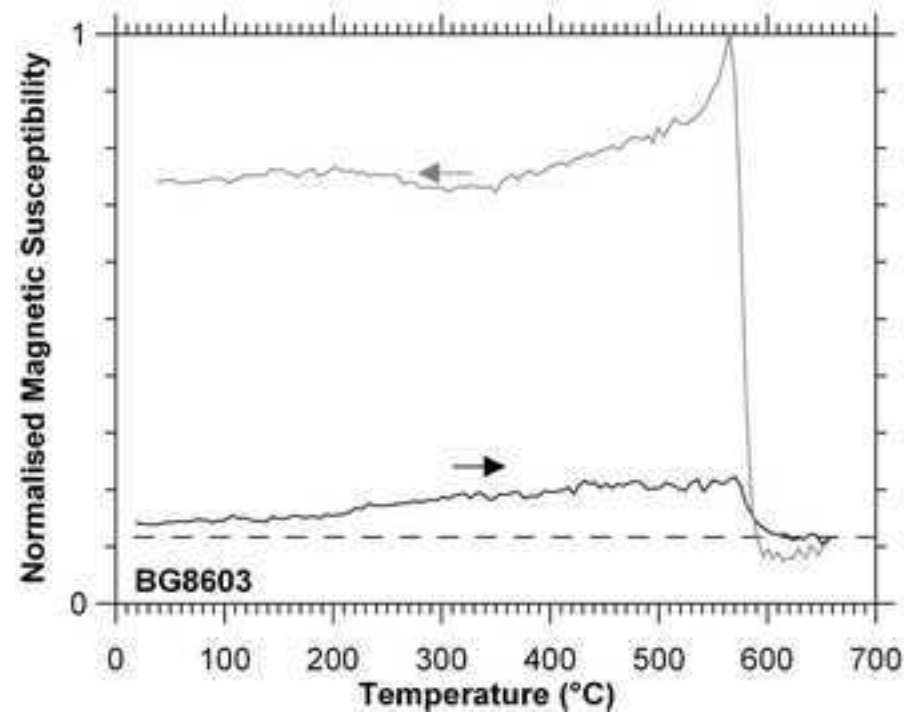
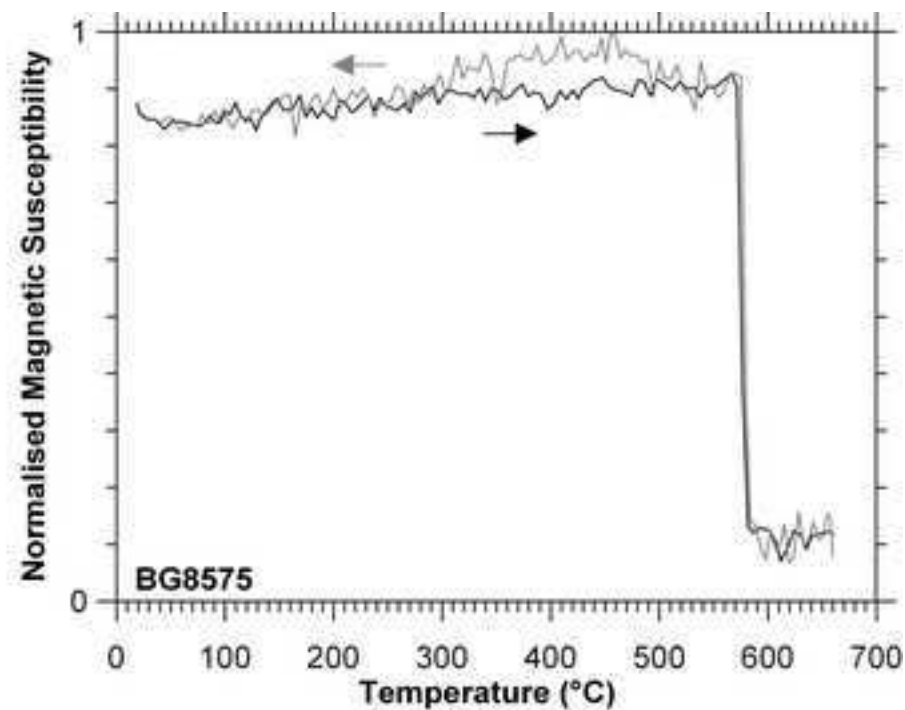
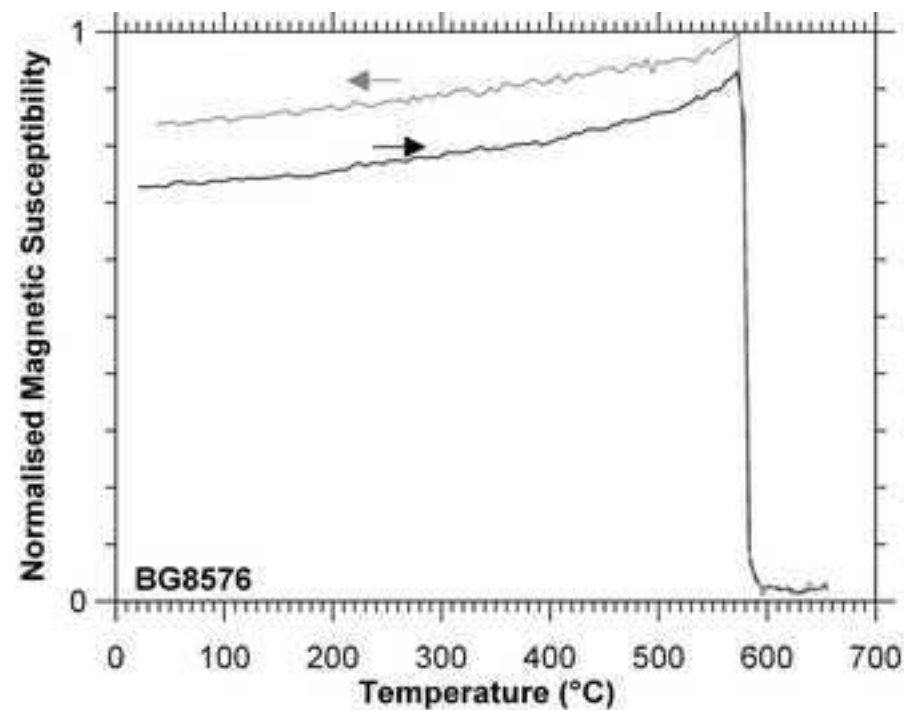


Figure 7 revised
[Click here to download high resolution image](#)

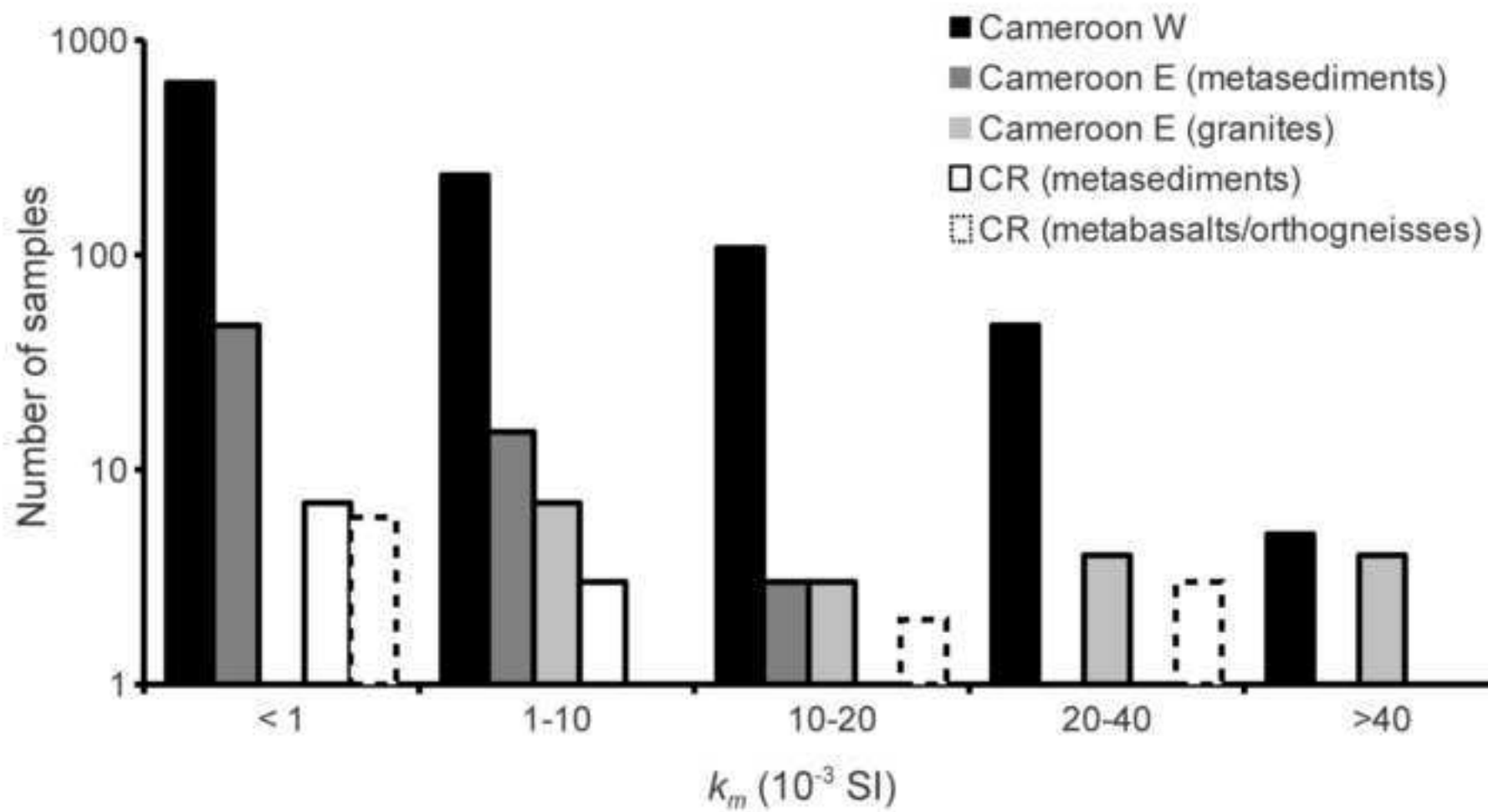
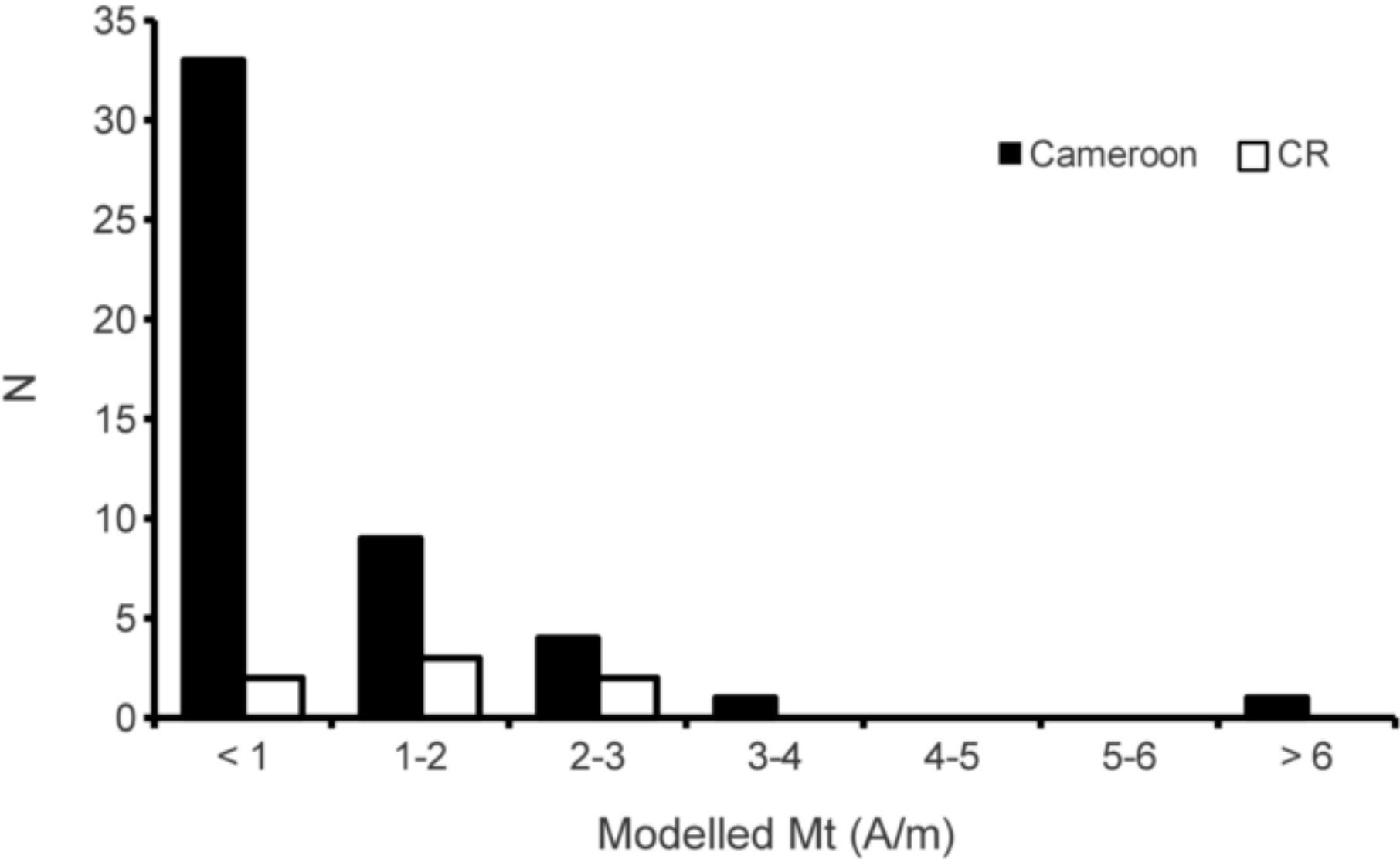


Figure 8 new
[Click here to download high resolution image](#)



1 **Table 1.** Magnetization* and density contrasts of the best models for the source of the BMA.

<i>Layer**</i>	<i>k</i> (10 ⁻³ SI)	NRM (A/m)	d (g.cm ⁻³)	<i>Rock type***</i>
1	10	4.0	2.870	<i>Magnetic source layer</i>
2	1	-	3.000	<i>Metabasalt</i>
3	1	-	2.900	<i>Granulite/Orthogneiss</i>
4	1	-	2.850	<i>Amphibolite</i>
5	1	-	2.665	<i>Quartzite</i>
6	1	-	2.630	<i>Schist</i>
7	1	-	2.640	<i>Panafrican nappe</i>
8	-	-	3.300	<i>Mantle rocks</i>

2 *all layers have their magnetization oriented in the 1960 (I= -14.5°, D=-5°) and 2011 (I= -16.76°, D=0.3°)
3 magnetic field directions in Bangui for the modelling of the ground and satellite magnetic data, respectively.
4 **see correspondance in Figure 3.
5 ***these rock types are expected with regards as their densities, their magnetization properties and the surface
6 geology.

1 **Table 2.** Magnetic properties of rock samples from the Bangui area.

<i>Lithology</i>	ID	χ	NRM	Mt	Q	NRM/SIRM	Laboratory modelled	<i>Sampling site</i>
		(10 ⁻⁹ m ³ .kg ⁻¹)	(A.m ² .kg ⁻¹)	(A/m)		(%)	Mt (A/m)	
<i>Itabirite</i>	8603	798	23856.2	76.4	1117.8	43.6	88.1	<i>Bogoin</i>
	243	629	237.5	0.8	14.1	5.1	7.5	<i>Bogoin</i>
<i>Migmatite</i>	8576	12201	2041.1	6.4	6.3	7.6	2.3	<i>Mabo</i>
	8575	8496	66.0	0.8	0.3	0.7	1.1	<i>Mabo</i>
<i>Orthogneiss</i>	240	85	833.8	2.3	365.5	53.1	2.1	<i>Mabo</i>
	234	229	342.8	0.9	55.9	36.1	1.5	<i>Sibut</i>
	235	5165	102.7	0.7	0.7	3.4	0.5	<i>Sibut</i>
	216	23	0.9	0.0	1.4	-	-	<i>Galabadjia</i>
<i>Granodiorite</i>	8632	7587	382.9	1.6	1.9	1.6	1.8	<i>La Mbi</i>
<i>Metaperidotite</i>	8840	5223	76.7	0.6	0.5	0.8	0.9	<i>La Mbi</i>
	8838	1235	105.6	0.4	3.2	-	-	<i>La Mbi</i>
	8836	164	3.0	0.0	0.7	-	-	<i>Sibut</i>
<i>Quartzite</i>	203	1902	82.7	0.4	1.6	-	-	<i>Boali</i>
	8564	5	1.4	0.0	11.0	-	-	<i>Bossembélé</i>
	213	7	0.8	0.0	3.8	-	-	<i>Mbalki</i>
	452	20	0.4	0.0	0.7	-	-	<i>Ouango</i>
<i>Granulite</i>	230	304	38.8	0.1	4.8	-	-	<i>Sibut</i>
<i>Metabasalt</i>	8602	292	0.2	0.0	0.0	-	-	<i>Bogoin</i>
<i>Micaschist</i>	249	171	2.2	0.0	0.5	-	-	<i>Boali</i>
<i>Metasilexite</i>	217	52	1.3	0.0	0.9	-	-	<i>Kamaro</i>

<i>Cipolin</i>	8631	-1	0.4	0.0	-11.9	-	-	<i>Fatima</i>
	8610	-1	0.4	0.0	-13.0	-	-	<i>Ndjimba</i>

Supplementary Material (new)

[Click here to download Supplementary Material: SupplementaryMaterial.pdf](#)